Impact ejecta emplacement on terrestrial planets

Gordon R. Osinski [a,b,*], Livio L. Tornabene [c], Richard A.F. Grieve [a,b,d]

[a] Departments of Earth Sciences/Physics and Astronomy, University of Western Ontario, 1151 Richmond Street, London, ON, Canada N6A 5B7
[b] Canadian Lunar Research Network/NASA Lunar Science Institute, Canada
[c] Center for Earth and Planetary Studies, National Air and Space Museum, Smithsonian Institution, Washington, DC 20560-0315, USA
[d] Earth Sciences Sector, Natural Resources Canada, Ottawa, ON, Canada K1A 0E8

ABSTRACT

Impact cratering is one of the most fundamental processes responsible for shaping the surfaces of solid planetary bodies. One of the principal characteristics of impact events is the formation and emplacement of ejecta deposits, an understanding of which is critical for planetary exploration. Current models of ejecta emplacement, however, do not account for several important observations of ejecta deposits on the terrestrial planets, in particular, the presence of more than one layer of ejecta. Furthermore, there is also no universal model for the origin and emplacement of ejecta on different planetary bodies. We present a unifying working hypothesis for the origin and emplacement of ejecta on the terrestrial planets, in which the ejecta are emplaced in a multi-stage process. The generation of the continuous ejecta blanket occurs during the excavation stage of cratering, via the conventional ballistic sedimentation and radial flow model. This is followed by the emplacement of more melt-rich, ground-hugging flows – the "surface melt flow" phase – during the terminal stages of crater excavation and the modification stage of crater formation. Minor fallback occurs during the final stages of crater formation. Several factors will affect the final morphology and character of ejecta deposits. The volatile content and cohesiveness of the uppermost target rocks will significantly affect the runout distance of the ballistically emplaced continuous ejecta blanket, with impact angle also influencing the overall geometry of the deposits (e.g., the production of the characteristic butterfly pattern seen in very oblique impacts). Ejecta deposited during the surface melt flow stage is influenced by several factors, most importantly planetary gravity, surface temperature, and the physical properties of the target rocks. Topography and angle of impact play important roles in determining the final distribution of surface melt flow ejecta deposits with respect to the source crater. This working hypothesis of ballistic sedimentation and surface melt flow provides a framework in which observations of ejecta at impact craters can be compared and placed in the context of the respective terrestrial planets.

© 2011 Elsevier B.V. All rights reserved.

1. Introduction

Meteorite impact craters represent an important geological landform in the solar system and are among the highest priority scientific targets for the international exploration of the Moon and Mars (e.g., Barlow, 2010; Hiesinger and Head, 2006). It has become apparent over the past two decades that meteorite impact events also have played an important role throughout Earth's history, shaping the geological landscape, affecting the evolution of life (e.g., Kring, 2000) and producing economic benefits (e.g., Grieve, 2005). Despite the ubiquitous occurrence of impact craters, however, important aspects of the processes and products of their formation remain poorly constrained. One such process is the emplacement of impact ejecta deposits and the provenance of their components, in particular,

impact melt. As with all impactites, the record on Earth is the only source of ground truth data on ejecta. An understanding of impact ejecta deposits and their components is critical for the results of planetary exploration, particularly future sample return missions. Their compositional and physical characteristics provide fundamental information about the sub-surface of planets. A prime example is on Mars, where the presence of so-called fluidized (or layered) ejecta deposits was the initial evidence to infer the presence of subsurface ice (e.g., Carr et al., 1977).

This contribution synthesizes field and laboratory data on Earth impact products and structures and combines them with planetary remote sensed observations. These provide the input for a working hypothesis for the origin, nature and emplacement of ejecta around simple and complex impact craters on the terrestrial planets. We do not discuss multi-ring basins here due to a current lack of observations and overall understanding of their formation. It should also be noted that current numerical simulations are unable to reproduce all the observations from planetary impact craters in terms of ejecta deposits (Artemieva et al., 2009). Some recent work has

* Corresponding author at: Departments of Earth Sciences/Physics and Astronomy, University of Western Ontario, 1151 Richmond Street, London, ON, Canada N6A 5B7. Tel.: +1 519 661 4208; fax: +1 519 488 4721.
E-mail address: gosinski@uwo.ca (G.R. Osinski).

started to address this but, to-date, the published simulations have focused on the emplacement of very distal ejecta deposits related to the K–Pg impact (Artemieva and Morgan, 2009; Goldin and Melosh, 2009). A driving paradigm of this work is that the overall processes involved in the generation of impact ejecta and crater-fill deposits and their *initial* emplacement are, in principle, essentially the same on all the terrestrial planets. Planetary gravity, atmospheric, and target properties have secondary, but important, effects on the nature of ejecta and account for detailed differences in ejecta between the terrestrial planets. We briefly discuss the unique Martian scenario of impacts that involve appreciable ground ice in the target, but note that a complete discussion is outside the scope of this paper. In support of the working hypothesis, we first present some critical observational evidence from the terrestrial planets.

2. Critical observations from the terrestrial planets

Impact ejecta deposits are defined here as any target materials, regardless of their physical state, that are transported beyond the rim of the *transient* cavity formed directly by the cratering flow-field (Fig. 1a, b). In complex craters, therefore, ejecta deposits occur in the crater rim region interior to the final crater rim. We focus on proximal ejecta deposits, which are, by definition, found within 5 crater radii of the source crater (Stöffler and Grieve, 2007). Fresh impact craters on all the terrestrial planets are typically surrounded by a "continuous ejecta blanket" that extends approximately 1 to 2 crater radii beyond the crater rim (Melosh, 1989). This continuous ejecta blanket is thickest at the rim. Beyond this, the deposits are typically thin and patchy. For a full discussion of the characteristics of continuous ejecta blankets (e.g., structural rim uplift, overturned flaps, and clast size distributions, etc.), the reader is referred to Chapter 6 in Melosh (1989).

### 2.1. The Moon and Mercury

Continuous ejecta blankets around lunar craters are typically blocky and of high albedo, when fresh (Melosh, 1989). Radial textures and patterns are common and the ejecta blanket thins with increasing radial distance. The maximum diameter of boulders in an ejecta blanket increases with crater size (Bart and Melosh, 2007). It is generally acknowledged that the continuous ejecta blanket, and proximal ejecta deposits in general, on airless bodies, such as the Moon and Mercury, are emplaced *via* the process of ballistic sedimentation. The ballistic emplacement of primary crater-derived ejecta produces secondary cratering, which results in the incorporation of local material (secondary ejecta) in the primary ejecta, via considerable modification and erosion of the local external substrate.

The characteristics of this ballistic sedimentation model for proximal ejecta, namely increasing source depth and incorporation of secondary local substrate materials with increasing radial range (Oberbeck, 1975), are a tenet in the interpretation of lunar samples (Heiken et al., 1991). A typically overlooked, but critical, observation is that proximal ejecta may consist of more than one layer.

The Moon represents an end-member case with respect to the terrestrial planets. Low planetary gravity and lack of atmosphere result in cratering efficiency, for a given impact, that is higher than on the other terrestrial planets. Cratering efficiency is defined as the ratio of the mass of the target displaced to the mass of the impactor (Melosh, 1989). As a portion of the transient cavity formed in an impact event that is due to the excavation of target materials, the cratering efficiency of equivalent impacts (same sized and type of impactor, same type of target and same impact velocity) is relatively lower on planetary bodies with higher surface gravities. Similarly, as gravity is an acceleration and acts to retard excavation, cratering efficiency is relatively lower for larger impact events (i.e., more time is required to complete excavation) on the same planet, given equivalent impact velocity and impactor and target types.

Planetary gravity has little effect on the volume of impact melt produced in a given impact event, beyond its effect on impact velocity (Grieve and Cintala, 1997). As a result, the relative volume of impact melt to transient cavity on the Moon is the lowest among the terrestrial planets for a given-sized cavity (Cintala and Grieve, 1998). Nevertheless, what is generally interpreted to be impact melt ponds on the rim terraces of complex lunar craters and overlying parts of the continuous ejecta blanket have been documented since the 1970s (Hawke and Head, 1977; Howard and Wilshire, 1975) (Fig. 2A,B). The interpretation is that these generally flat and smooth surfaced ponds consist of impact melt that has flowed and pooled according to local slopes, after its initial emplacement as ejecta. More recently, the Lunar Reconnaissance Orbiter Camera (LROC) has captured spectacular images of impact melt forming ponds and veneers within the crater interior and the terraced crater rim region (Fig. 2C), overlying ballistic ejecta deposits (Fig. 2C,D), and draping central uplifts (Fig. 2E–G) within and around many complex lunar craters. These melt deposits show intricate surface textures and morphologies indicative of flow, such as channels and arcuate cracks and ridges. Such impact melt deposits also are visible in radar imagery, where they appear to be associated with larger craters (>40 km in diameter) (Campbell et al., 2010). For craters formed from oblique impact, such as the 85 km diameter Tycho crater, it is apparent that more melt is present in the downrange direction (Hawke and Head, 1977).

With the increased resolution provided by LROC, it is apparent that some small, simple craters also preserve dark deposits consistent with
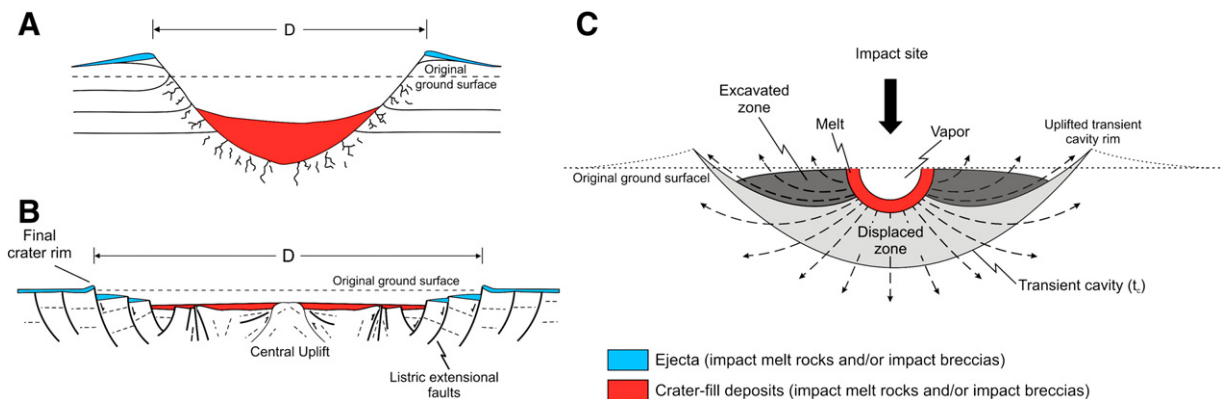
Fig. 1. Typical schematic cross sections of simple and complex craters and of a transient cavity. A. Simple impact crater. B. Complex impact crater. Note that ballistic ejecta is present inside the crater rim because it originates from the transient cavity, which is largely destroyed during crater collapse. Also note that typical cross sections, such as this, in the literature, do not show multiple ejecta layers. "D" represents the rim (or final crater) diameter, which is defined as the diameter of the topographic rim that rises above the surface for simple craters, or above the outermost slump block not concealed by ejecta for complex craters (Turtle et al., 2005). C. Theoretical cross section through a transient cavity showing the locations of impact metamorphosed target lithologies. Modified from Melosh (1989).
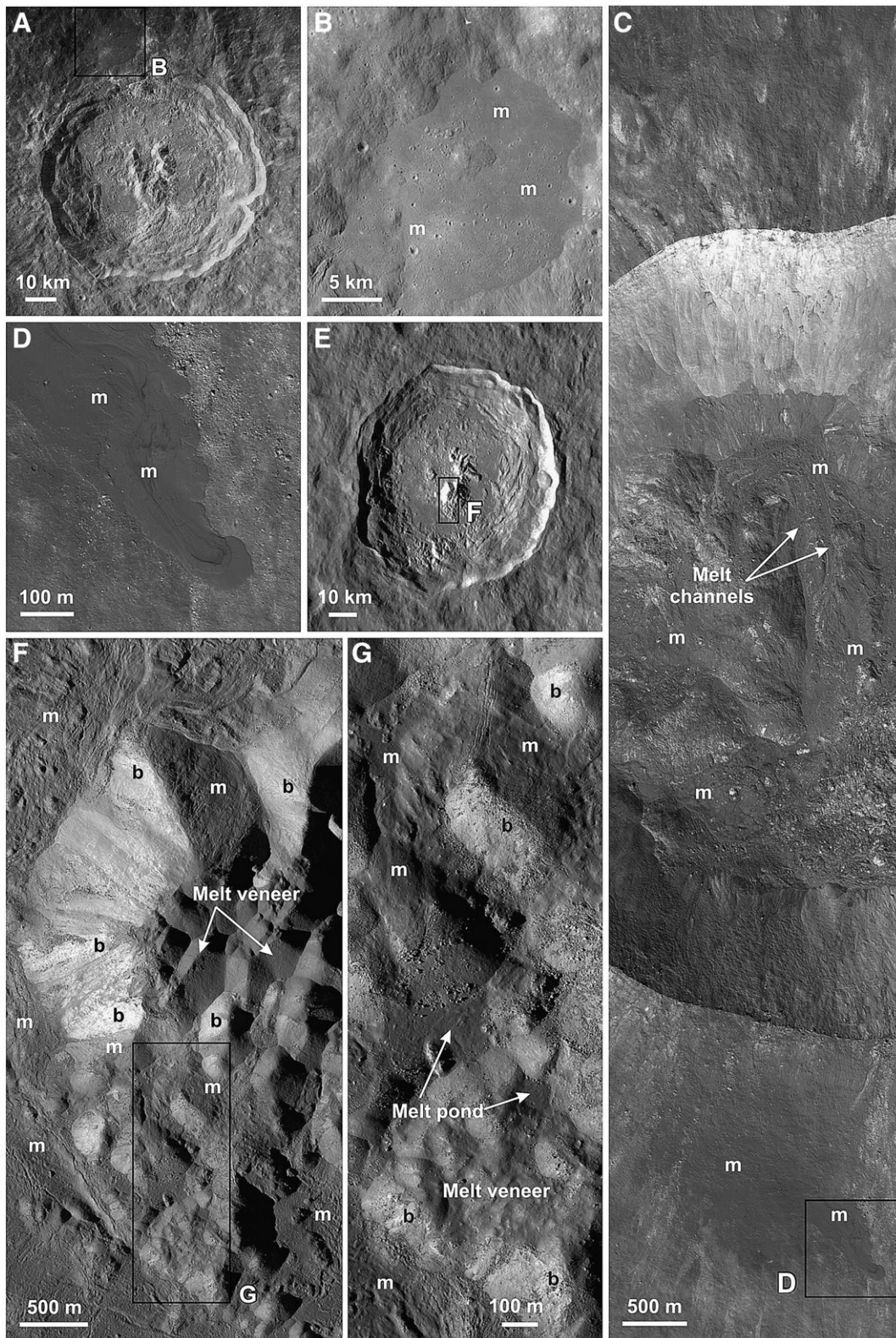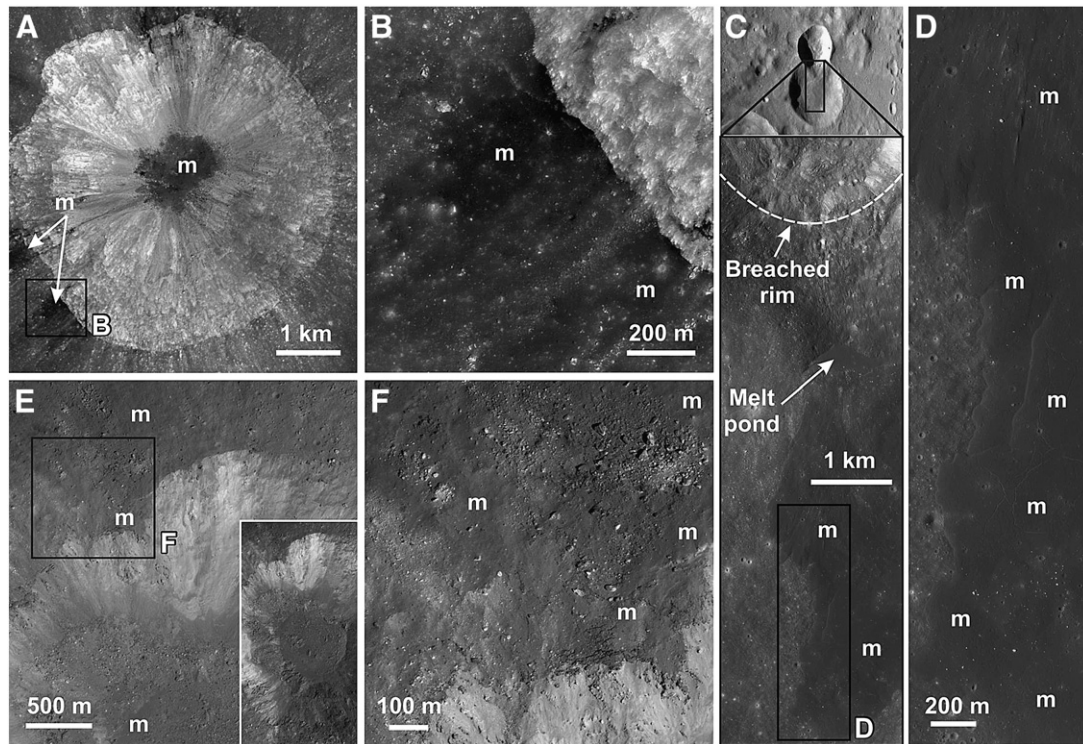
Fig. 2. Observations of complex lunar craters. A. and B. Apollo 16 image of the 76 km diameter King Crater Large showing a large impact melt ("m") pond (B). Portions of Apollo 16 image 1580 (NASA). C. A portion of LROC NAC image pair (M106209806RE) of melt within the interior and overlying the continuous ejecta blanket at the 22 km diameter Giordano Bruno crater (NASA/GSFC/ASU). D. A close-up from (C) showing melt overlying the lighter blocky ballistic ejecta, with evidence for flow from the top left to the bottom right. E. An LROC WAC image (M103223292MC) of the 71 km diameter Jackson Crater providing context for (F) and (G) (NASA/GSFC/ASU). F. A portion of the left LROC NAC image pair (M10322391LE) of the central uplift shows the presence of impact melt draping the anorthositic bedrock ("b") of the central uplift (NASA/GSFC/ASU). G. A close-up from (F) shows smooth veneers of impact melt draping the central uplift.

being impact melt (Fig. 3). These melt deposits can form small pools within the crater interior and form patchy veneers that clearly overlie the more blocky, brighter continuous ejecta blankets around crater rims (Fig. 3A,B,E, F). Fig. 3C and D shows an interesting example, to be discussed later, where a crater superposes an older crater and, as a result, the rim is breached to the south and a substantial portion of the

Fig. 3. Observations of simple lunar craters. A. and B. Blocky, ballistic ejecta deposits overlain by dark, patchy impact melt ("m") around a 5 km diameter simple crater. Portions of LROC NAC image M125733619. C. Context image and enlargement showing an ~15 km diameter simple crater that is superimposed on a larger more subdued crater. As a result, the rim of this younger crater is mostly missing in the region where the two craters overlap. In this crater, a substantial portion of the melt ("m") has escaped the transient cavity and is, instead, found as a large tongue-like melt body that extends into the older crater. Portion of LROC NAC image M105557749R. D. An enlargement of C) shows the thick, dark melt deposits ("m"), with likely cooling cracks, overlying an older cratered surface. Portion of LROC NAC image M105557749R. E. Image of a fresh 2.7 km diameter simple crater (see inset) with substantial deposits of melt ("m") within the crater interior and overlying the ballistic ejecta blanket. Portion of LROC NAC image pair M112162602LE. F. A close-up of E) shows a veneer of melt ("m") overlying the blocky ballistic ejecta blanket. The melt forms a crust around the rim of the crater in this region. All images NASA/GSFC/ASU.

melt has flowed out of the crater via the breach to form a tongue like body that extends to the south.

High resolution imagery, such as that provided by LROC, is not available for Mercury; however, images recently returned by the MESSENGER spacecraft show the presence of what is interpreted as melt ponds around several Mercurian impact craters (Prockter et al., 2010). Continuous ejecta blankets on Mercury are typically blocky and of high albedo, when fresh similar to lunar craters. If ballistic sedimentation followed by radial flow accounts for the emplacement of the continuous ballistic ejecta, it begs the question as to the origin, timing, and emplacement mechanism(s) of this overlying (melt-rich) ejecta observed around many lunar and Mercurian craters.

2.2. Venus

Venus is the antithesis of the Moon. The relatively high planetary gravity and thick atmosphere reduce cratering efficiency for a given impact relative to the Moon (Schultz, 1993), while the higher average impact velocity and high ambient temperature of the target rocks increase the relative efficiency of impact melting (Grieve and Cintala, 1997). In addition, any entrained clastic debris in the impact melt is hotter than on the Moon, resulting in higher thermal equilibrium temperatures, lower viscosities, and longer cooling time for the impact melt deposits (Grieve and Cintala, 1995). This relative increase in the amount (a factor of greater than 6) and nature of impact melt lithologies produced for a given transient crater size compared to the Moon is manifest as spectacular melt outflows exterior to Venusian craters (Asimow and Wood, 1992) (Fig. 4). Melt outflows are most common in craters resulting from oblique impacts and in larger structures (Chadwick and Schaber, 1993). Larger structures have reduced cratering efficiency relative to impact melt production compared to smaller impacts (Grieve and Cintala, 1995). While

oblique impacts result in relatively less melt production, they also result in reduced cratering efficiency, such that the volume of melt generated relative to transient cavity volume increases slightly with decreasing impact angle, except at low angles (<15°) where there is a dramatic drop in melt volume (Pierazzo and Melosh, 2000). An additional factor in relative melt production and thus potential volume of impact melt outflows at any given crater on Venus, is impact velocity, with model calculations indicating a doubling of melt production over a velocity range of 10 km s^{-1} (the escape velocity of Venus) and 45 km s^{-1} (Alpert and Pierazzo, 2000).

In detail, the outflows from impact craters on Venus display some diversity. Asimow and Wood (1992) recognized erosive, channel-
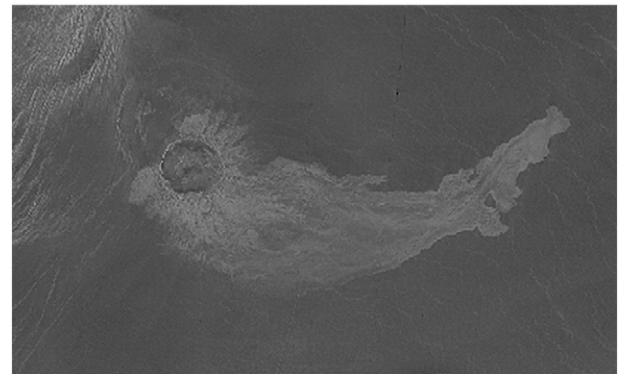
Fig. 4. Magellan image of the 90 km diameter Adams crater, Venus (56.10°S, 98.90°E). Many of the outflows have a proximal portion that have higher and more uniform radar backscatter than the continuous ejecta and a well-defined boundary between them, suggesting a discrete stratigraphic boundary. The distal portions of the outflows may extend several crater diameters, are more radar dark (suggesting less entrained clastic blocks) and flow down-slope, following the local topography (Chadwick and Schaber, 1993).

forming outflows of what was probably impact melt that may consist of a mix of solid and melt. In some cases, the former flows uphill (downrange from the crater) initially before turning downhill and following the local topographic slope (e.g., at the 48 km Parra crater). This attests to an initial emplacement mode that was highly energetic. Three dimensional numerical simulations of the outflows separated them into two types: "catastrophic" outflows originating at or near the rim, with outflow rates of 10^{10} m³/s lasting less than 100 s, and "gentle" outflows originating in the ejecta, with outflow rates of 10^4 m³/s lasting more than 10^5 s (Miyamoto and Sasaki, 2000). The emplacement of the catastrophic outflows was attributed directly to the cratering process, while that of the gentle outflows was attributed to secondary segregation and drainage of melt materials from within previously emplaced ejecta.

2.3. Mars

Data returned from spacecraft and surface missions over the past several years have shown that Mars is the most Earth-like planetary body in the solar system. In the context of the current study, it is important to highlight the complex and often volatile-rich nature of the Martian crust, which makes it similar to Earth but unlike the Moon, Mercury or Venus, and the presence of a thin atmosphere. Perhaps unsurprisingly, the Martian impact cratering record (Strom et al., 1992) is notably more diverse than that of the Moon, Mercury or Venus. In particular, approximately one-third of all Martian craters ≥5 km in diameter possess discernable ejecta blankets, with over 90% possessing so-called layered ejecta that display single (SLE; 86%), double (DLE; 9%), or multiple (MLE; 5%) layer morphologies (Barlow, 2005) (Fig. 5). In general, MLE craters are typically larger and their ejecta are found at greater radial distances than SLE craters, when normalized to crater size. So-called ramparts or ridges, the origin of which is debated, are often seen at the outer edge(s) of the ejecta layers. DLE craters remain enigmatic but are most common in mid-latitude regions (Barlow, 2006). It is widely accepted that layered ejecta deposits were highly fluidized at the time of their emplacement and occurred as relatively thin ground-hugging flows (Carr et al., 1977). Contrasting models have been proposed to account for these layered ejecta on Mars: the interaction of ballistic ejecta with a volatile-rich vapor plume (Carr et al., 1977), interaction with the Martian atmosphere (Schultz and Gault, 1979), or a combination of the two (Barlow, 2005; Komatsu et al., 2007).

Recent high-resolution imagery of relatively pristine Martian impact craters provides some important new constraints and observations. Some Martian craters are very lunar-like in terms of crater interior and ejecta morphology. One of the best examples is the Pangboche crater, which is located on the flank of Olympus Mons at ~21 km elevation (Fig. 5A). At such an altitude, it is not possible for volatiles to be present either in the atmosphere or the target rocks. In terms of impact melting on Mars, some workers have suggested that the volumes of impact melt produced are small, except in the largest of impacts (Pope et al., 2006). However, recent imagery shows the presence of impact melt deposits forming large bodies and/or ponds on crater floors (Fig. 5A,B), terraces (Fig. 5A,B), and overlying continuous ejecta blankets (Fig. 5B–D). Images of other, larger craters show impact melt deposits flowing off central uplifts (Fig. 5E–I), as observed at lunar craters. Impact melt flows also have been recently documented on the interior walls of the well-preserved Tooting crater (Morris et al., 2010). It should be noted that all of these examples are from fresh, relatively dust-free impact craters. It is predicted that such melt deposits are likely to be more common but are typically obscured by dust or other post-impact deposits in the majority of young craters, or eroded in older craters.

2.4. Earth

The impact cratering record on Earth provides the only ground-truth data for the lithological and structural character of impact structures. Thus, any model must be consistent with the interpreta-tion of the characteristics of ejecta deposits on Earth if it is to be generally applicable. The high levels of geological activity, however, result in the very poor preservation of exposed ejecta on Earth. There are two known cases where impact melt rocks occur outside the rim in terrestrial simple craters: Tenoumer, Mauritania and Pingualuit (formerly New Quebec), Canada (Table 1). At Tenoumer, they occur as three groups of isolated, 1–2 m high outcrops, which are up to 200 m long, and were described originally as intrusive dikes when it was believed that the crater was the result of the collapse of a magmatic dome (Monod and Pomerol, 1966). The contacts between the melt rocks and the country rocks are not visible due the ubiquitous sand cover in the area (Fudali, 1974). At Pingualuit, the melt rocks occur as a few isolated cobbles of float found up to 3.5 km north of the rim (Marvin and Kring, 1992). The rounded nature of the samples is indicative of fluvial transport but they were not transported from an original location within the crater by glacial action, as the northern half of the crater was ice free (Bouchard and Saarnisto, 1989). No breccia deposits, which could represent ballistic ejecta, have been recognized at either Tenoumer or Pingualuit. At the Lonar and Barringer Craters, impact melt-bearing breccias have been identified in the ejecta deposits (Maloof et al., 2010; Osinski et al., 2006), but no impact melt rocks to date.

The nature, lithological and stratigraphic relations of ejecta at several buried complex structures are known only from drill core but indicate the presence in the proximal ejecta of a low-shock, lithic breccia overlain by a melt-bearing deposit (Table 1). The range of target rocks suggests that this trait is not due to the effect of volatiles, layering, or other effects of target lithology on the impact cratering process. Some of the best-preserved and exposed ejecta deposits on Earth occur at the Ries structure, Germany (Engelhardt, 1990). The Ries clearly displays a distinctive two-layer ejecta configuration (Fig. 6A) with a series of impact melt-bearing breccias (suevites) and minor impact melt rocks overlying the continuous ejecta blanket (Bunte Breccia). Studies of the Bunte Breccia strongly support the concept of ballistic sedimentation. The Bunte Breccia has material from two main sources: primary ejecta excavated from the transient cavity (average ~31 vol.%), and local secondary ejecta (average ~69 vol.%, but >90% at large radial distances) (Hörz et al., 1983). The incorporation of large amounts of secondary ejecta (Hörz et al., 1983), deformation (Kenkmann and Ivanov, 2006) and radially-oriented striations on the pre-impact target surface, very poor sorting (clasts from mm to km in size), and overall low shock level of Bunte Breccia deposits are evidence that the ejecta moved radially outwards as some form of ground-flow after initial ballistic ejection (Fig. 6B). This is consistent with observations at the similarly-sized 23-km-diameter Haughton structure, Canada (Osinski et al., 2005), and the smaller simple 1.2-km-diameter Barringer (Grant and Schultz, 1993) (USA) and 1.8-km-diameter Lonar (Maloof et al., 2010) (India) craters (Table 1). The sharp contact between the Ries ejecta layers (Fig. 6A) indicates that there is a clear temporal hiatus between emplacement of the ballistic Bunte Breccia and the overlying suevites/impact melt deposits (Hörz, 1982).

Early workers suggested that the upper surficial "suevite" ejecta at the Ries was deposited sub-aerially from an ejecta plume (Engelhardt, 1990; Engelhardt and Graup, 1984) and the term "fallout" was used to qualify the suevites; the crater-fill suevites were called "fallback" suevites. This is despite the fact that the surficial suevites are unsorted to poorly sorted (Fig. 6A,C,D), which is not predicted by subaerial deposition (i.e., fallout from an ejecta plume). Such deposits are typically sorted and display normal grading, as is the case in pyroclastic fall deposits (Fisher and Schmincke, 1984). The origin of the surficial suevite as the result of fallout from an ejecta plume over the crater is not supported by recent numerical models (Artemieva et al., 2009). What may be true "fall" deposits do occur in the central crater cavity of the Ries structure in the form of a ~17 m thick unit that displays moderate grading (Stöffler, 1977).

Based on field and scanning electron microscopy observations, it has been suggested that the proximal surficial suevites were
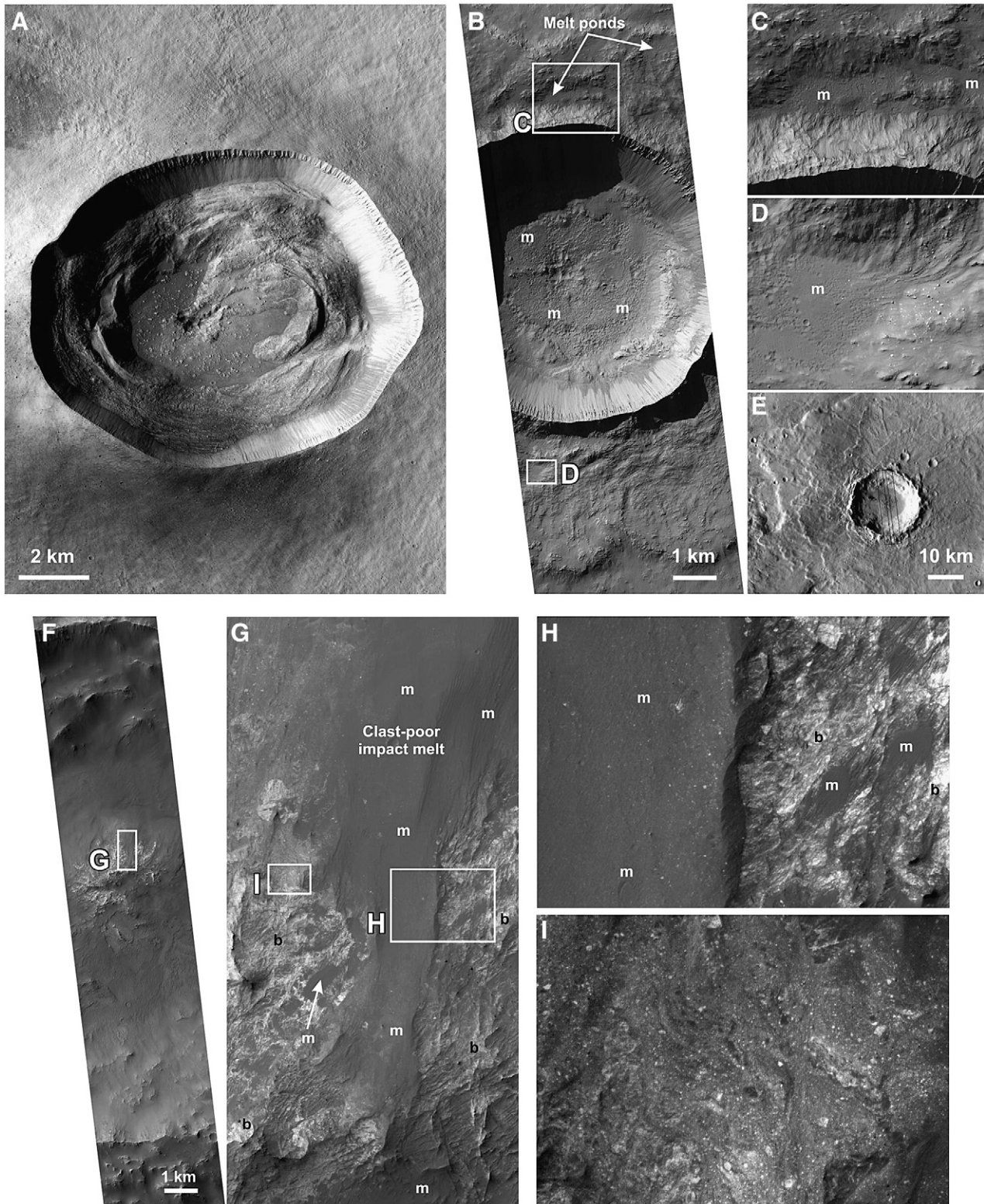
Fig. 5. Images of Martian impact craters. A. Image of the 11 km diameter Pangboche Crater, situated near the summit of Olympus Mons. Portion of CTX image P02_001643_1974_XN_17N133W (NASA/JPL/MSSS). B. HiRISE image PSP_008135_1520 (NASA/JPL/UA) showing a fresh unnamed 7 km diameter impact crater in Hesperia Planum (108.9° E, 27.9° S) and providing context for (C) and (D). This crater displays characteristic pitted materials likely representing impact melts (Tornabene et al., 2007) ("m") in the crater interior and exterior (observed as pitted and ponded deposits on the ejecta blanket). Without HiRISE imagery, this crater would be misclassified as an SLE crater. C. and D. The pitted ponds form in topographic depressions and there is clear evidence for in-flow and some remobilization of these materials after their initial emplacement in various locations near the rim and off the distal rampart. E. An image provided by the global mosaic of THEMIS daytime TIR imagery of a well-preserved 20 km diameter complex crater (43.4° E, 24.3°S), which provides context for (F–I); NASA/JPL/ASU. F. HiRISE image PSP_007109_1555 provides a more detailed swath through the impact crater (NASA/JPL/UA). G. Close-up view showing a close-up of the central portion of the crater that reveals the partially exposed bedrock of the crater central peak (lighter-toned materials) and what we interpret to be draped and injected impact melt flows and breccias (darker-toned materials) (NASA/JPL/UA). H. and I. Close-ups showing spectacular clast-poor (H) and clast-rich (I) impact melts ("m") draping and flowing off the light toned bedrock ("b") exposed in the central uplift.

Table 1
Compilation of preserved ejecta deposits around impact structures on Earth.

Crater	Buried	Apparent crater diameter, D_a (km)	Rim diameter, D (km)	Target stratigraphy[a]	Ejecta description	Maximum depth of excavation of lower ballistic ejecta	Depth of excavation of upper melt-rich ejecta
Barringer	N	N/A	1.2	Sst, Slt, Lst, Dol	Continuous ballistic ejecta blanket with evidence for ground hugging flow following ballistic emplacement (Shoemaker, 1963), which produced flow lobes (Grant and Schultz, 1993). Small mm- to cm-sized glassy beads occur as lag deposits overlying the continuous ejecta blanket (Hörz et al., 2002), which contain minor volumes of impact melt-bearing breccias (Osinski et al., 2006).	0.08 D	N/A
Bigach	N	8	?	Sst, Slt, Vol	Ejecta poorly exposed and studied. They are polymict breccias with blocks up to ~20 m across (Masaitis, 1999); it is not clear if any melt or shock effects are present.	Unknown	Unknown
Boltysh	Y	24	?	Gr, Gn	Ejecta deposits very poorly exposed and eroded in close proximity to the crater rim. In the Tyasmin River valley ~6–8 km outside the crater rim, low shock, melt-free "monomict" breccias are overlain by polymict breccias (Gurov et al., 2003). Both breccias comprise crystalline rocks; polymict breccias contain more highly shocked material. The polymict breccias are described as "lithic breccias" but they also are reported as containing altered melt particles (Gurov et al., 2003).	Unknown	Unknown
Chicxulub	Y	N/A	180	Gr, Gn overlain by ~3 km of Lst, Dol, Evap	The Chicxulub ejecta deposits vary with distance from the crater. Close to the crater, the UNAM-7 drill core (located 126 km from the crater center) shows a two-layer stratigraphy with melt-free to poor lithic breccias and megabreccias derived from the sedimentary cover overlain by melt-rich impact melt-bearing breccias (suevites) with abundant crystalline basement clasts (Salge, 2007). The lower sedimentary breccias are interpreted as ballistic ejecta and have been compared with the Bunte Breccia at the Ries structure (Salge, 2007). At greater distances, the ballistic ejecta comprises largely locally derived secondary ejecta (Schönian et al., 2004).	0.017 D	Unknown
Haughton	N	23	16	Gn and Gr overlain by 1.9 km Lst, Dol, minor Evap, Sst, Sh	Remnants of the ejecta blanket are preserved in the SW of the Haughton impact structure. There, a two-layer sequence of pale yellow–brown melt-poor impact breccias and megablocks overlain by pale gray clast-rich impact melt rocks are preserved (Osinski et al., 2005). The former are derived from depths of >200 to <760 m and are interpreted as the continuous ballistic ejecta blanket (cf., the Bunte Breccia at the Ries structure). The pale gray impact melt rocks are derived from deeper levels.	0.80 km = 0.035 D_a = 0.05 D	~2 km = 0.08 D_a = 0.12 D
Lonar	N	N/A	1.9	Bs	Continuous ballistic ejecta blanket; evidence for ground hugging flow following ballistic emplacement (Maloof et al., 2010). Possibly at the transition of "simple ballistic emplacement and ballistic sedimentation" (Maloof et al., 2010). Impact spherules are found in many locations with rarer samples of melt-bearing rocks.	Unknown	Unknown
Mistastin	N	28	?	An, Gr, Mn	Ejecta deposits are preserved in the crater rim region where a complex series of melt-free and -poor lithic impact breccias are overlain by impact melt-bearing breccias and coherent silicate impact melt rocks (Mader et al., 2011).	Unknown	Unknown
New Quebec (Pingualuit)	N	N/A	3.4	Gn	Ejecta largely eroded. Isolated melt samples are found as float beyond the N rim. The glacial direction is to the SE (Bouchard and Saarnisto, 1989), therefore, it is highly improbable that the melt samples originated from inside the crater cavity. They are interpreted as melt "splashes"	Unknown	Unknown
Obolon	Y	18 (poorly constrained)	?	Gn and Gr overlain by ~300 m of Sst, Clt, Lst	A borehole (# 467) close to the crater rim contains a two-layer ejecta sequence: a 22.5 m thick series of melt-free lithic breccias, comprising clays with glide planes, are overlain by a 14 m thick sequence of impact melt-bearing impact breccias with clasts from the crystalline basement (Gurov et al., 2009).	~300 m 0.017 D_a	>300 m
Ragozinka		9	?	Folded Lst, Bs, Sst, Sh overlain by 100–200 m of Sst, Slt	Ejecta very poorly exposed and preserved. An "outlier" near the village of Vostochnyi comprises a series of low shock polymict breccias with clasts up to ~7 m in size (Vishnevsky and Lagutenko, 1986). Lower contacts are not exposed and the upper surface is erosional.	Unknown	Unknown
Ries	N	24	?	Gn, Gr overlain by 500–800 m of Sst, Sh, Lst	A two two-layer sequence of ejecta is preserved at the Ries structure with melt-free to poor Bunte Breccia overlain by impact melt-bearing breccias (suevites) (Engelhardt, 1990). The Bunte Breccia largely comprises largely sedimentary rocks derived from depths of <850 m in the target stratigraphy; whereas the suevites are largely derived from the deeper levels in the target. An occurrence of impact melt rock at Polsingen lies in the same stratigraphic position as the suevites (i.e., overlying Bunte Breccia) (Osinski, 2004).	0.85 km = 0.035 D	>800 m
Tenoumer	N	N/A	1.9	Gn and Gr overlain by 20–30 m of Lst	The continuous ejecta blanket is partially exposed and comprises mm- to m-size blocks of the crystalline basement. "Impact melt rock occurs in patches outside the crater" overlying the continuous ejecta blanket, predominantly to the E, NW, and SW (Pratesi et al., 2005).	Unknown	Unknown

[a]Abbreviations: An = anorthosite, Bs = basalt, Dol = dolomite, Evap = evaporite, Gr = granite, Gn = gneiss, Lst = limestone, Mn = mangerite, Sh = shale, Slt = siltstone, Sst = sandstone, Vol = mixed extrusive volcanic rocks.

Fig. 6. Terrestrial impact melt-bearing impactites. A. Two layered ejecta stratigraphy at the Ries impact structure, Germany (Aumühle Quarry, 3 km inside the NE crater rim). Impact melt-bearing breccias, or "suevites" (s) overlie Bunte Breccia (BB). Note the sharp contact between the two units. This is indicative of a hiatus in ejecta deposition and necessitates a two stage ejecta emplacement model. The height to the top of the outcrop is ~8 m. B. Large blocks of Malm limestone within the Bunte Breccia at the Gundelsheim Quarry, 7.5 km outside the NE crater rim. The height to the top of the outcrop is ~9 m. The poor sorting, low shock level and modified pre-impact target surface (smooth area at bottom of image) are consistent with ballistic sedimentation and subsequent radial flow (Hörz et al., 1983). The inset shows the contact between the Bunte Breccia and the underlying limestone displaying characteristic striations ("Schliff-Fläche"). C. Elongate, "aerodynamically-shaped" glass bombs (arrow) aligned parallel to the suevite — Bunte Breccia contact. This is consistent with surface flow. 40 cm long rock hammer for scale. D. Close up of the suevite showing a glass ("g") particle with delicate fingers (arrow) of glass extending into the groundmass, consistent with the glass being partially molten during transport and deposition. 7 cm wide lens cap for scale. E. Elongate, "aerodynamically-shaped" glass bombs and gneiss-cored glass "bombs". These features are widely cited as *de facto* evidence for airborne emplacement but these are actually from a dike of suevite in the crater floor of the Mistastin impact structure, Labrador, shown in (F). 7 cm wide lens cap for scale. F. Dike of suevite ~2 m across. Note the person for scale on the horizon in the upper right. G. Close-up view of the dike showing the alignment of elongate glass clasts with the walls of the dyke (compare to C). 7 cm wide lens cap for scale. H. View toward the rim of extensive deposits of coherent impact melt rock ("m") overlying impact melt-bearing breccias ("s") in the crater rim region of the Mistastin structure. Elongate, "aerodynamically-shaped" glass bombs and gneiss-cored glass "bombs" are present in these breccias but, as with the overlying melt rocks, they were never airborne.

emplaced as surface flow(s), either comparable to pyroclastic flows or as ground-hugging volatile- and melt-rich flows (Bringemeier, 1994; Newsom et al., 1986; Osinski et al., 2004). Evidence for the flow origin includes the lack or sorting (Fig. 6A,C,D), the preferred orientation of glass clasts with the Bunte Breccia contact (Fig. 6C) (Bringemeier, 1994; Hörz, 1965; Meyer et al., in press), and the presence of chilled margins at the bottom and, where preserved, at the top of some

outcrops (Engelhardt, 1967), which suggests that suevites were deposited as a single unit. Deposition temperatures in excess of 900 °C and the presence of various impact melt phases in the groundmass, with evidence for flow or deformation following deposition (Fig. 6D), further suggest that these flows were melt-rich and that these melts were partially molten during transport (Osinski et al., 2004). A flow origin also has been suggested for the relatively rare coherent impact

melt rocks that reside atop the Bunte breccia, at the Ries (Osinski, 2004).

The most intransigent arguments used to support an airborne origin for suevites at the Ries are melt glass clasts, similar in shape to "fladen" (German for "round, flat dough cake") and "gneiss-cored glass bombs" (Fig. 6C,D) (e.g., Engelhardt, 1990; Stöffler, 1977). While airborne transportation was offered as a possible explanation for their shape (Engelhardt, 1990), the term "fladen" has morphed over the years into "aerodynamic-shaped" in English texts. Similar characteristics have been described from "suevites" at several impact structures, where they are offered as *de facto* evidence that these materials were airborne (Masaitis, 1999). Examples of melt glass "fladen", however, can be found in dikes of impact melt-bearing breccia that are injected into the floor of the Mistastin structure, Canada (Fig. 6E–G). In this case, the "fladen" shaped melt glass clasts are due to shaping during transport in a confining flow. Melt glass coatings on lithic clasts can occur as the clasts are rotated during transportation in the presence of melt, which is also the case for the dike at Mistastin (Fig. 6E). Similar observations were made at the Manicouagan structure, Canada, in the 1970s (Currie, 1972) and are characteristic of the melt-bearing breccias that lie beneath coherent impact melt rocks, such as at the Mistastin (Fig. 6H) and Manicouagan structures. As with the respective coherent melt rocks, these breccias with melt "fladen" below the melt rocks were never airborne, with their melt glass morphologies the result of flow. The image shown in Fig. 6H is particularly informative as this is taken from the crater rim region at Mistastin, where a series of impact breccias are overlain by impact melt rocks that preserve evidence for flow (Mader et al., 2011). These melt rocks and underlying breccias are ejecta deposits, by definition, and they lie in the same stratigraphic position as impact melt ponds seen in the terraced region of complex lunar craters.

3. Synthesis

3.1. Generation of continuous ejecta blankets

Current models of the impact cratering process only consider the formation of a continuous ejecta blanket and discrete crater-fill deposits (Melosh, 1989; Oberbeck, 1975). It is generally accepted that impact craters entail the generation of a transient cavity (Dence, 1968; Grieve and Cintala, 1981; Melosh, 1989), regardless of their final size, morphology and on what planetary body they form. This cavity consists of an upper "excavated zone" and a lower "displaced zone" (Fig. 1C). Target materials within the upper zone are ejected beyond the transient cavity rim to form the continuous ejecta blanket. These materials are derived from the excavated zone of the transient cavity and are of generally relatively low shock level (Hörz, 1982). It is well understood that the initial emplacement of a continuous ejecta blanket is via the process of ballistic sedimentation (Oberbeck, 1975); subsequent secondary cratering, incorporation of local external substrate materials in the primary ejecta and radial flow result in considerable modification of the primary ejecta and erosion of the local external substrate. As such, the main parameters that will affect the overall nature, distribution, and runout distance of the ballistically emplaced continuous ejecta blanket, will be the volatile content and cohesiveness of the uppermost target rocks (Table 2).

Target materials within the displaced zone are accelerated initially downward and outward to form the base of the expanding cavity (Grieve et al., 1977; Stöffler et al., 1975). The bulk of this displaced zone comprises target rocks that are shocked to relatively low to intermediate shock levels and they ultimately come to form the parautochthonous rocks of the true crater floor in simple and complex craters and the central uplifted structures, in the case of complex

Table 2
Parameters affecting the final morphology of ejecta deposits for a given planetary body.

Parameter	Effect(s) on ballistic ejecta generation and emplacement	Effect(s) on melt generation and emplacement
Impact angle	The angle of impact affects the *distribution* of ballistic ejecta with respect to the source crater, with the preferential downrange concentration of ejecta at angles <60°, the development of a "forbidden zone" uprange of the crater at angles of <45°, and, finally, at very low angles of <20°, the development of a second "forbidden zone" downrange of the crater, leading to the characteristic "butterfly" pattern (Gault and Wedekind, 1978).	Melt-rich materials are preferentially emplaced downrange, driven by both the displacement of the cratering flow field and the migration of the uplifting crater floor in this direction.
Impact velocity	Scaling relationships exist between impact velocity and the range of ballistic ejecta (Housen and Holsapple, 2011).	Increased melt volumes for the same transient crater size.
Volatile content of surface materials	Volatile-rich surficial materials will result in greater "fluidization" of secondary ejecta, leading to increased runout.	None.
Cohesiveness of surface materials	Less cohesive rocks on surface will result in greater incorporation of secondary ejecta, leading to increased runout and fluidization.	None.
Composition of target rocks in the melt zone	Minor, as very little melt is contained in the ballistic ejecta.	The onset of melting porous and volatile-bearing targets (typically sedimentary rocks but not necessarily) is much lower (e.g., ~20 GPa in porous sandstones) (Kieffer et al., 1976). For H_2O-bearing planetary bodies, ice, and in some cases liquid water, must also be considered; recent calculations suggest that H_2O ice will undergo complete melting at ~2–4 GPa depending on temperature (Stewart and Ahrens, 2005). Thus, much more melt will be generated for the same pressures and temperatures than a dry crystalline target. This will result in proportionally more melt in the displaced melt-rich zone of the transient crater and, thus, a more fluidized and voluminous overlying melt-rich ejecta layer.
Size of crater	Scaling relationships exist between crater size and the range of ballistic ejecta (Housen and Holsapple, 2011).	Relatively, more melt is produced in larger craters with respect to crater size (Cintala and Grieve, 1998; Grieve and Cintala, 1992, 1995). This affects the volume and thickness of interior and exterior impact melt-bearing deposits and, thereby, their morphologies and possibly composition.
Topography	Minor, as ballistic sedimentation greatly modifies pre-impact topography.	Following the cessation of large-scale crater collapse and central uplift formation, the melt-rich materials will flow relative due to both crater-related and pre-impact topography. This essentially tends to form both a large central intra-crater deposit (i.e., allochthonous crater-fill) and ponds in depressions within the near-rim ejecta, wall-terraces and distal ballistic ejecta deposits. The pre-impact topography will control to a large extent the distribution of melt ponds around a crater. For example, if a crater rim intersects a pre-existing topographic low, melt will preferentially escape the transient cavity in this region to form larger, localized exterior melt ponds.

craters. Some allochthonous, highly shocked and melted materials are driven down into the transient cavity and along curved-paths parallel to the expanding and displaced floor of the transient cavity. The bulk of these melt-rich materials does not leave the transient cavity and, ultimately, forms the allochthonous crater-fill deposits in simple and complex impact structures (Grieve et al., 1977; Melosh, 1989).

3.2. Generation of multiple layers of melt-rich ejecta

With the above as the current tenet, observations of craters on the terrestrial planets require a modified model for the origin and emplacement of impact melt lithologies and the formation of impact ejecta and crater-fill deposits. Based on the above observations that impact melt deposits, or what is generally interpreted as impact melt in the planetary context, occurs outside the rim at both simple and complex craters, we suggest that the current view of impact ejecta emplacement, i.e., a one-stage process occurring during the excavation stage, is incomplete. A multi-stage emplacement process that intimately links the generation of impact melt lithologies, allochthonous crater-fill deposits and ejecta is required. We now discuss the various parameters that could be responsible for this multi-stage emplacement process, before presenting a summary of the working hypothesis in Section 4.

3.2.1. Initial melt production and early emplacement

In simple craters, there is movement of highly shocked and melted materials initially down into the expanding transient cavity. The observation of thin melt veneers around some simple lunar craters (e.g., Fig. 3B, E) and impact melt rocks outside the rim at some terrestrial craters indicates that some of the melt-rich materials from the displaced zone of the transient cavity are driven up and over the transient cavity walls and rim region. This process will be particularly important for oblique impacts, where the sub-surface flow field is displaced downrange (Anderson et al., 2004). Except in exceptional circumstances, the bulk of the melted material lining the transient cavity, however, remains within the cavity and moves inward as the transient cavity walls collapse inward, where they become intercalated with the brecciated cavity wall materials to form the internal breccia lens partially filling simple craters (Grieve and Cintala, 1981). Exceptions include cases where a crater may superpose an existing crater (Fig. 3C, D) or some other large topographic feature (e.g., deep canyons), resulting in breached crater rims. A particularly informative exception to this rule is shown in Fig. 3C and D, where most of the melt in one crater has flowed out of the crater due to the breaching of this crater rim where it superposes an older crater. Instead of flowing back into the crater, the low elevation of the transient cavity rim in this region allowed a substantial portion of the melt, which would normally be mostly contained within the crater fill, to escape and flow outwards. On a larger scale, a similar situation may have occurred during the formation of the ~150 km diameter Oudemans Crater, Mars, where a large amount of the crater fill escaped the crater and in-filled valleys of the Valles Marineris system to the north (Mest et al., 2011).

While this process of cavity wall collapse and mixing with impact melted material is an established tenet of cratering mechanics at simple craters (e.g., Melosh, 1989), the relatively late escape of some impact melt over the rim is not explicitly stated. It is suggested that two main parameters will affect this phase of ejecta emplacement; namely, the angle of impact and the initial volume of impact melt generated (Table 2).

3.2.2. Late-stage melt emplacement

Notwithstanding the minor emplacement of melt outside of crater rims by the cratering flow field discussed above, the observations of relatively extensive impact melt-rich deposits overlying ballistic ejecta deposits and the sharp contact between these units, where observed, argue for the general late-stage emplacement of melt-rich ejecta. In larger complex craters – where these melt-rich deposits are most abundant – central structural uplift occurs, as the transient

cavity walls collapse to form a relatively shallow crater-form. Field observations and numerical models suggest that central uplifts partially collapse to varying degrees depending on crater-size and target properties (Collins et al., 2002; Osinski and Spray, 2005). In some cases, this uplift may originally overshoot the original target surface and then collapse (Collins et al., 2002). It is possible that cavity modification, in particular uplift, thus imparts an additional outward momentum to the melt- and clast-rich lining of the transient cavity during the modification stage, resulting in flow toward and over the collapsing crater rim and onto the proximal ballistic ejecta blanket, forming a second thinner and potentially discontinuous layer of non-ballistic ejecta. This offers an explanation for the presence of melt-rich materials stranded on top of the central peaks and terraces of complex lunar (Fig. 2F,G) and Martian (Fig. 6F–I) and terrestrial (Tong et al., 2010) craters and impact melt ponds within and outside of the crater rim region of all terrestrial planets (Figs. 2A–D, 5B–D, 6H). It should be noted that the second, upper layer may be thin and discontinuous and not easily observable from spacecraft. A perfect example of this is that many SLE craters on Mars, with high-resolution imagery, can be seen to have patchy melt-rich deposits (Fig. 5B–D) (Tornabene et al., 2007). This mechanism will also be important for oblique impacts, where field (Scherler et al., 2006) and numerical modeling (Ivanov and Artemieva, 2002; Shuvalov, 2003) studies suggest that the horizontal momentum of the impactor is preserved into the final stages of crater formation such that there is an uprange initiation of crater rim collapse and the migration of the uplifting crater floor downrange.

For oblique impacts, an additional mechanism may be the emplacement of external melt deposits in a process more akin to what is believed to occur at simple craters, i.e., by the late-stages of the cratering flow-field. In this case, the initial direction of the flows is preferentially downrange. Indeed some of the most notable melt outflows from complex craters on Venus are associated with craters formed from oblique impacts (Chadwick and Schaber, 1993). This also may the case for the Ries impact on Earth, where the only *bona fide* impact melt rocks are found outside the inner ring on the inner slope of the eastern rim, in keeping with "the preferred flow of melt downrange" (Stöffler et al., 2002). Model calculations indicate that, although the volume of melt is lower in oblique impacts, the fraction of melt that is retained in the transient cavity is also less (Ivanov and Artemieva, 2001). They also show that the cratering flow-field is asymmetric, with higher down-range velocities, but that subsequent cavity modification is much more symmetric (Ivanov and Artemieva, 2001). Thus, it would appear that preferential initial direction of external melt flows in oblique impacts may be related to asymmetries in the cratering flow-field in addition to subsequent modification processes.
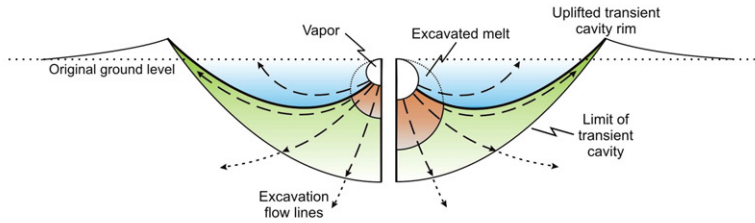
3.2.3. Final complications

It is clear that other factors can govern the final resting place of these late-stage melt-rich deposits, the most important of which is the local topography of the target region. Impact melt-rich materials will continue to flow for an extended period of time following impact and, thus, will tend to follow topography and collect in topographic lows (Fig. 2A,B, and Fig. 3C,D). A spectacular example of this effect is King Crater on the Moon, where there would likely be no enormous external melt pond if it were not for the size and proximity of the pre-existing crater that now contains this melt pond (Fig. 2A,B). Recent interpretations of LROC images of external melt flows around lunar complex craters also indicate a multi-stage influx of melt into flows and drainage from central peaks for a substantial time (a few weeks) following crater formation (Bray et al., 2010).

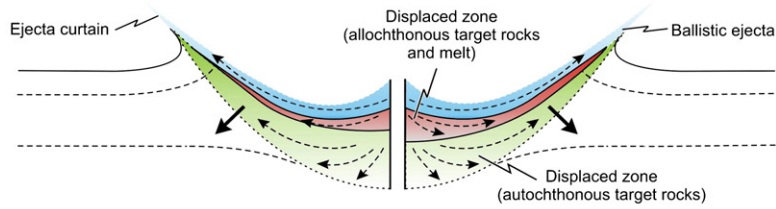### 4. The working hypothesis

A multi-stage working hypothesis for the origin and emplacement of impact melt lithologies and the formation of impact ejecta and crater-fill deposits is proposed (Fig. 7), based on a synthesis of the
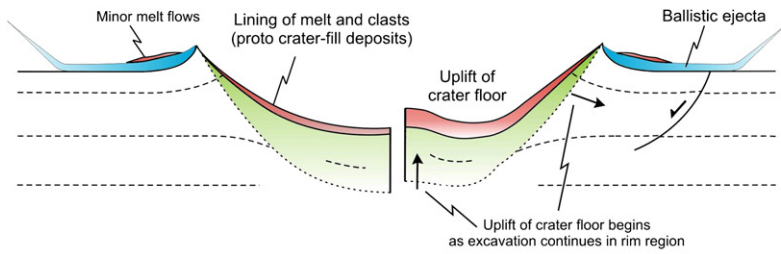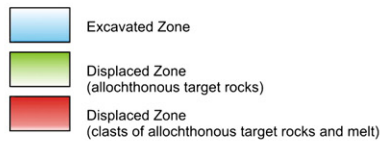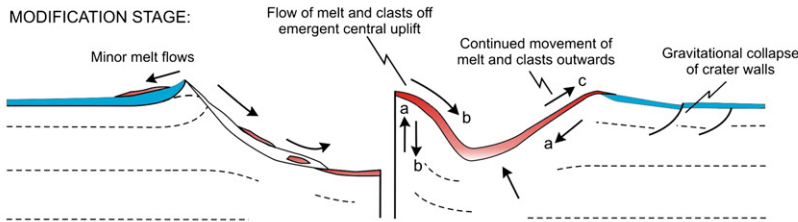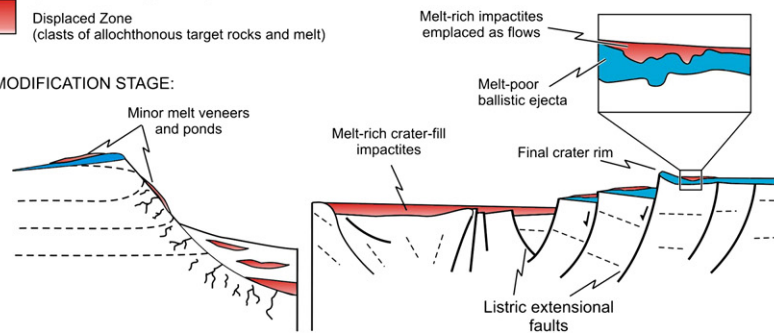
Fig. 7. Model for the formation of impact ejecta and crater fill deposits. This multi-stage model accounts for melt emplacement in both simple (left panel) and complex craters (right panel), as described in the text. It should be noted that this is for a "typical" impact event. As discussed in the text, the relative timing and important of the different processes can vary, particularly for more oblique impacts. It should be noted that in the modification stage section, the arrows represent different time steps, labeled "a" to "c". Initially, the gravitational collapse of crater walls and central uplift (a) results in generally inwards movement of material. Later, melt and clasts flow off the central uplift (b). Then, there is continued movement of melt and clasts outwards once crater wall collapse has largely ceased (c).

interplanetary observations presented herein. As with the crater-forming process in general – and its subdivision into contact and compression, excavation, and modification – we note that ejecta emplacement will be a continuum and that the different emplacement processes will overlap in time. This will be important in larger craters, where models show that uplift of the transient cavity floor

commences before outward growth and excavation of the transient cavity ceases in the rim region (Kenkmann and Ivanov, 2000; Stöffler et al., 1975).

1) *Crater excavation and ballistic emplacement* — The initial emplacement of a continuous ejecta blanket is via the process of ballistic sedimentation (Fig. 7), with subsequent radial flow (Oberbeck, 1975). Materials are derived from the excavated zone of the transient cavity and are of generally relatively low shock level (Hörz, 1982).

2) *Late excavation–early modification and minor flow emplacement* – In simple craters, minor amounts of highly shocked and melted materials are driven up and over the transient cavity walls and rim region (Fig. 7), consistent with the presence of thin melt veneers around some simple lunar craters and impact melt rocks outside the rim at some simple terrestrial craters. This process is particularly important for oblique impacts, where the sub-surface flow field is displaced downrange (Anderson et al., 2004), and impacts into varied topography, which form breached rims.

3) *Crater modification and* "late" *flow emplacement* — The generation of large-scale impact melt-rich deposits overlying ballistic ejecta deposits most likely occurs largely during the modification stage of crater formation (Fig. 7). The momentum necessary to emplace these deposits may come from two sources. First, cavity modification, in particular uplift, can impart an additional outward momentum to the melt- and clast-rich lining of the transient cavity during the modification stage, resulting in flow toward and over the collapsing crater rim and onto the proximal ballistic ejecta blanket, forming a second thinner and potentially discontinuous layer of non-ballistic ejecta. This process will become more important as crater size and melt volume increases. For oblique impacts, an additional mechanism is the emplacement of external melt deposits in a process more akin to what is believed to occur at simple craters, i.e., by the late-stages of the cratering flow-field. In this case, the initial direction of the flows is preferentially downrange. The specific amount and distribution of external melt-rich deposits on a given terrestrial planet will be influenced by several parameters (Table 2), the most important being variations in the volatile content of surface materials and the relative size of the melt zone to that of the crater. The final resting place for the melt-rich deposits will be controlled to a large extent by the local topography of the target region. Subsequent remobilization following impact also may occur (Bray et al., 2010).

4) *Minor fallback* — Fallback of material from the vapor-rich ejecta plume will occur during the final stages of crater formation and will produce the very minor "fallback" material in the crater interior, which will be characteristically graded, such as observed at the Ries structure in the terrestrial environment (Pernicka et al., 1987). The presence of thin (few meters), fine-grained ejecta haloes extending beyond the continuous ejecta blanket of lunar, Venusian, and Martian craters also is consistent with the late-stage settling out of micrometer to millimeter size fines from the ejecta plume (Ghent et al., 2010).

We note that the actual internal flow mechanisms responsible for transport of ejecta, and the formation of features such as ramparts around some Martian craters, are not addressed in this paper and remain a topic of debate. Other authors have addressed these questions with various explanations being proposed (e.g., Barnouin-Jha et al., 2005; Mouginis-Mark and Baloga, 2006; Oberbeck, 2009; Suzuki et al., 2007; Wada and Barnouin-Jha, 2006). It is hoped that with this new working hypothesis for impact ejecta emplacement in hand, solutions for these other poorly understood aspects of ejecta deposits will be forthcoming.

5. Implications

5.1. Differences between the terrestrial planets

In summary, our working hypothesis is that this model for the *initial* emplacement of ejecta and crater-fill deposits should be applicable for all impact events on any planetary body. It is suggested that variations in gravity, surface temperature, and the relative size of the melt zone to that of the crater can account for the major differences in crater ejecta morphology between the Moon (and Mercury) and Venus. This model provides an explanation for the presence of melt ponds and flows around lunar and Mercurian craters and for their much greater extent and size around Venusian craters.

In addition to these factors, we suggest that on geologically complex bodies, such as Mars and Earth, the volatile content of surface materials and the properties of impact melt generated from volatile-rich targets may account for some of the observed differences with respect to craters on the Moon, Mercury, and Venus. A complete discussion of this is outside the scope of this contribution, however, we note, for example, that double layered ejecta craters are most common in the northern plains of Mars, where ground-ice is thought to also be more common and voluminous in the subsurface. In our working hypothesis, the uppermost layer of double layered ejecta craters could represent an extreme version of the isolated melt ponds seen in lunar craters (Fig. 1), in some Martian craters (Fig. 5A–C) and the melt-rich ejecta deposits at the Ries (Fig. 6A) and Haughton structures. The reason for the presence of a continuous second layer in some Martian craters may be that in ice-rich terrains, increased melt volumes (i.e., water from ice) will be produced, with ice melting at shock pressures of ~2.5–4.1 GPa (Stewart and Ahrens, 2005), thereby increasing the fluidization of the second layer of ejecta. Further work is planned on this topic. Finally, as discussed above, it should be noted that other parameters, in particular the velocity and angle of impact and the topography of the surface affect the final morphology of ejecta at individual craters.

5.2. Ejecta properties

One of the predictions of this multi-stage ejecta working hypothesis is that material in the upper, second layer of ejecta will be derived from deeper levels in the target (i.e., from the displaced zone of the transient cavity) and will contain more highly shocked and shock-melted material (because it comprises more of the melt zone; see Fig. 7) than the initial ballistic ejecta. If the target is compositionally stratified, then a compositional difference between the ejecta layers should be discernable. This is not a prediction of previous models for layered ejecta on Mars. Fig. 8A and B presents a clear case for Mars where, based on the regional stratigraphy (Rogers et al., 2005), the upper layer of ejecta is derived from a deeper ultramafic-rich level, compared to the lower mafic ballistic ejecta blanket. Another example of this compositional difference in ejecta layers is also observed at the Yalgoo crater (Tornabene et al., 2008).

Similar observations have been made at the Haughton and Ries impact structures on Earth, where two-layer ejecta deposits are preserved, with the upper layers being more melt-rich and derived from deeper levels than the lower ballistic ejecta (Osinski et al., 2005) (see Table 1 for other examples). Note that the suevite at the Ries is not a coherent melt flow, due to the physical differences in the final impact melt products from crystalline targets (Moon and Venus) and mixed sedimentary–crystalline targets (Ries) (Osinski et al., 2008). On the Moon, the lack of knowledge about the shallow structure of the crust makes it difficult to test this hypothesis, but the observations of lunar craters showing that the ballistic ejecta contains little or no melt but the second layer of ejecta is melt-rich (i.e., melt ponds), is consistent with this working hypothesis.
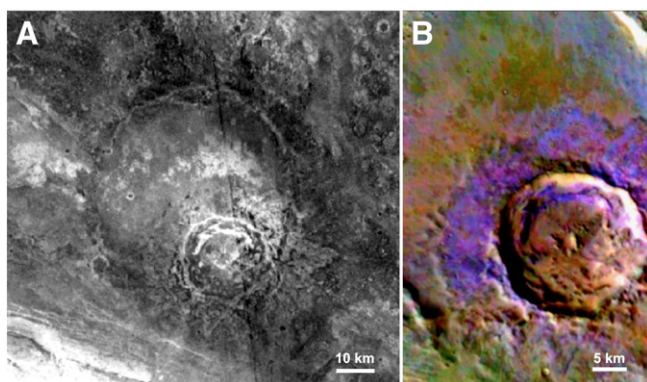
Fig. 8. A. An image provided by the global mosaic of THEMIS daytime TIR imagery of a 18 km diameter crater within a 42 km diameter crater slowing a DLE morphology (NASA/JPL/ASU). Relative thermal inertias, as interpreted from the pre-dawn temperature differences with respect to this crater, suggest that the outer ejecta lobe is coarser-grained than the inner one, which is consistent with observations of the DLE Ries structure. B. In addition, the two ejecta layers are compositionally distinct (as observed in this decorrelation stretched THEMIS TIR 8-7-5 radiance composite (NASA/JPL/ASU): the outer ejecta faces (orange) have a more "basaltic" composition, while the inner ejecta (blue) layer has a more "ultramafic" composition (consists predominately of clinopyroxene and olivine [~70%]; see (Rogers et al., 2005)). This ejecta blanket configuration is consistent with the "basaltic" materials originating from the near-subsurface and the "ultramafic unit" from a deeper unit underlying the "basaltic unit". This stratigraphy is also consistent with the regional noncrater exposed stratigraphy in this area (Rogers et al., 2005). (For interpretation of the references to color in this figure legend, the reader is referred to the web version of this article.)

5.3. Sampling planetary crusts

An estimate of the depth of excavation is critical for determining the provenance of planetary surface samples, which are not *in situ*, by virtue of an impact event. Very little ground-truth data exists to estimate depth of excavation (d_e), as few terrestrial craters preserve ejecta deposits and/or have the distinct pre-impact stratigraphy necessary for determining depth of materials (Table 1). Various estimates for the d_e are in the literature (Melosh, 1989). Based on stratigraphic considerations, d_e at Barringer Crater is >0.08D (Shoemaker, 1963), where D is the final rim diameter. Importantly, the depth and diameter of large complex craters and basins must be referred back to the "unmodified" transient cavity to reliably estimate the depth of excavation (Melosh, 1989). The transient cavity, however, is essentially destroyed during the modification stage of complex crater formation. The maximum d_e of material in the ballistic ejecta deposits of the Haughton and Ries structures, the only terrestrial complex structures where reliable data are available, yield identical values of 0.035 D_a (Table 1), where D_a is the apparent crater diameter. If the final rim diameter (D) is used, which is the parameter measured in planetary craters, a value 0.05 D is obtained for Haughton.

A critical consideration is that the upper layer of ejecta (and the crater-fill deposits) reflects the composition and depth of the displaced zone of the transient cavity (Fig. 1). At Haughton, this value is a minimum of 0.08 D_a or 0.12 D (Table 1). If sampling deeper-seated lithologies is the goal of future planetary sampling missions, these melt ponds could be prime exploration targets. Furthermore, these melt-rich ejecta are emplaced as relatively low-velocity ground hugging flows, with little incorporation of secondary ejecta. Thus, this ejecta is largely primary, unlike the ballistic ejecta. Melt ponds and flows in ejecta may, therefore, represent the most easily accessed and least ambiguous impact-derived products from a particular crater or basin.

6. Summary

It has become increasingly recognized over the past several years that impact cratering is one of the most fundamental geological processes in the solar system. In this contribution, we address one of the most important, yet poorly understood, aspects of the impact cratering process, namely the origin and emplacement of impact ejecta. We synthesize observations from all the terrestrial planets to develop a unifying working hypothesis for the origin and emplacement of ejecta on the terrestrial planets. This model accounts for several important observations of ejecta deposits, in particular the presence of more than one layer of ejecta, and also provides a universal model for the origin and emplacement of ejecta on different planetary bodies. We propose that ejecta are emplaced in a multi-stage process and not just during the excavation stage of crater formation as previously believed. In summary, the generation of the continuous ejecta blanket occurs during the excavation stage of cratering, via the conventional ballistic sedimentation and radial flow model as originally proposed by Oberbeck (1975). This is followed by the emplacement of more melt-rich, ground-hugging flows – which we term the "surface melt flow" phase – during the terminal stages of crater excavation and the modification stage of crater formation. Fallback is minor and occurs during the final stages of crater formation. We note that several factors will affect the final morphology and character of ejecta deposits, including the volatile content and cohesiveness of the uppermost target rocks, impact angle, and topography of the region surrounding the impact site.

In addition to providing a framework in which observations of ejecta at impact craters can be compared and placed in the context of the respective terrestrial planets, it is our hope that this new working hypothesis for the origin and emplacement of impact ejecta will aid in the interpretation of data from planetary exploration missions, including past and future sample return missions. Impact ejecta provide a unique window into the sub-surface of planetary bodies. As we show, craters with multiple layers of ejecta provide the potential to sample different depths in the target sequence with the uppermost melt-rich ejecta sampling the deepest levels in the stratigraphy.

References

Alpert, A., Pierazzo, E., 2000. Venusian impact melt production. Lunar Planet. Sci. 31 Abs. 1486.

Anderson, J.L.B., Schultz, P.H., Heineck, J.T., 2004. Experimental ejection angles for oblique impacts: implications for the subsurface flow-field. Meteorit. Planet. Sci. 39, 303–320.

Artemieva, N., Morgan, J., 2009. Modeling the formation of the K–Pg boundary layer. Icarus 201, 768–780.

Artemieva, N.A., Wünnemann, K., Meyer, C., Reimold, W.U., Stöffler, D., 2009. Ries Crater and suevite revisited: part II modelling. Lunar Planet. Sci. 40 Abs. 1526.

Asimow, P.D., Wood, J.A., 1992. Fluid outflows from Venus impact craters: analysis from Magellan data. J. Geophys. Res. 97, 13643–13665.

Barlow, N.G., 2005. A review of Martian impact crater ejecta structres and their implications for target properties. In: Kenkmann, T., Hörz, F., Deutsch, A. (Eds.), Large Meteorite Impacts III, Geological Society of America Special Paper 384. Geological Society of America, Boulder, pp. 433–442.

Barlow, N.G., 2006. Impact craters in the northern hemisphere of Mars: layered ejecta and central pit characteristics. Meteorit. Planet. Sci. 41, 1425–1436.

Barlow, N.G., 2010. What we know about Mars from its impact craters. Geol. Soc. Am. Bull. 122, 644–657.

Barnouin-Jha, O.S., Baloga, S., Glaza, L., 2005. Comparing landslides to fluidized crater ejecta on Mars. J. Geophys. Res. 110. doi:10.1029/2003JE002214.

Bart, G.D., Melosh, H.J., 2007. Using lunar boulders to distinguish primary from distant secondary impact craters. Geophys. Res. Lett. 34. doi:10.1029/2007GL029306.

Bouchard, M.A., Saarnisto, M., 1989. Déglaciation et paléo-drainages du cratère du Nouveau-Québec. In: Bouchard, M.A., Péloquin, S. (Eds.), L'Histoire naturelle du Cratére du Nouveau-Québec. Collection Environnement et Géologie, Université de Montréal, pp. 165–189.

Bray, V.J., Tornabene, L.L., Keszthelyi, L.P., Mcewen, A.S., Hawke, B.R., Giguere, T.A., Kattenhorn, S.A., Garry, W.B., Rizk, B., Caudill, C.M., Gaddis, L.R., Van Der Bogert,

C.H., 2010. New insight into lunar impact melt mobility from the LRO camera. Geophys. Res. Lett. 37. doi:10.1029/2010GL044666.

Bringemeier, D., 1994. Petrofabric examination of the main suevite of the Otting Quarry, Nordlinger Ries, Germany. Meteorit. Planet. Sci. 29, 417–422.

Campbell, B.A., Carter, L.M., Campbell, D.B., Nolan, M., Chandler, J., Ghent, R.R., Ray Hawke, B., Anderson, R.F., Wells, K., 2010. Earth-based 12.6-cm wavelength radar mapping of the Moon: new views of impact melt distribution and mare physical properties. Icarus 208, 565–573.

Carr, M.H., Crumpler, L.S., Cutts, J.A., Greeley, R., Guest, J.E., Masursky, H., 1977. Martian impact craters and emplacement of ejecta by surface flow. J. Geophys. Res. 82, 4055–4065.

Chadwick, D.J., Schaber, G.G., 1993. Impact crater outflows on Venus: morphology and emplacement mechanisms. J. Geophys. Res. 98, 20891–20902.

Cintala, M.J., Grieve, R.A.F., 1998. Scaling impact melting and crater dimensions: implications for the lunar cratering record. Meteorit. Planet. Sci. 33, 889–912.

Collins, G.S., Melosh, H.J., Morgan, J.V., Warner, M.R., 2002. Hydrocode simulations of Chicxulub Crater collapse and peak-ring formation. Icarus 157, 24–33.

Currie, K.L., 1972. Geology and Petrology of the Manicouagan Resurgent Caldera, Quebec, Geological Survey of Canada Bulletin 198. Geological Survey of Canada, Ottawa.

Dence, M.R., 1968. Shock zoning at Canadian craters: petrography and structural implications. In: French, B.M., Short, N.M. (Eds.), Shock Metamorphism of Natural Materials. Mono Book Corp, Baltimore, pp. 169–184.

Engelhardt, W.V., 1967. Chemical composition of Ries glass bombs. Geochim. Cosmochim. Acta 31, 1677–1689.

Engelhardt, W.V., 1990. Distribution, petrography and shock metamorphism of the ejecta of the Ries crater in Germany — a review. Tectonophys. 171, 259–273.

Engelhardt, W.V., Graup, G., 1984. Suevite of the Ries crater, Germany: source rocks and implications for cratering mechanics. Geol. Rundsch. 73, 447–481.

Fisher, R.V., Schmincke, H.U., 1984. Pyroclastic Rocks. Springer-Verlag, Berlin, p. 472.

Fudali, R.F., 1974. Genesis of the melt rocks at Tenoumer crater, Mauritania. J. Geophys. Res. 79, 2115–2121.

Gault, D.E., Wedekind, J.A., 1978. Experimental studies of oblique impacts. Proc. Lunar Planet. Sci. Conf. 9, 3843–3875.

Ghent, R.R., Gupta, V., Campbell, B.A., Ferguson, S.A., Brown, J.C.W., Fergason, R.L., Carter, L.M., 2010. Generation and emplacement of fine-grained ejecta in planetary impacts. Icarus 209, 818–835.

Goldin, T.J., Melosh, H.J., 2009. Self-shielding of thermal radiation by Chicxulub impact ejecta: firestorm or fizzle? Geology 37, 1135–1138.

Grant, J.A., Schultz, P.H., 1993. Degradation of selected terrestrial and Martian impact craters. J. Geophys. Res. 98, 11,025–11,042.

Grieve, R.A.F., 2005. Economic natural resource deposits at terrestrial impact structures. In: McDonald, I., Boyce, A.J., Butler, I.B., Herrington, R.J., Polya, D.A. (Eds.), Mineral Deposits and Earth Evolution. : Geological Society, London, Special Publications, 248. The Geological Society of London, London, pp. 1–29.

Grieve, R.A.F., Cintala, M.J., 1981. A method for estimating the initial impact conditions of terrestrial cratering events, exemplified by its application to Brent crater, Ontario. Proc. Lunar Planet. Sci. Conf. 12B, 1607–1621.

Grieve, R.A.F., Cintala, M.J., 1992. An analysis of differential impact melt-crater scaling and implications for the terrestrial impact record. Meteoritics 27, 526–538.

Grieve, R.A.F., Cintala, M.J., 1995. Impact melting on Venus: some considerations for the nature of the cratering record. Icarus 114, 68–79.

Grieve, R.A.F., Cintala, M.J., 1997. Planetary differences in impact melting. Adv. Space Res. 20, 1551–1560.

Grieve, R.A.F., Dence, M.R., Robertson, P.B., 1977. Cratering processes: as interpreted from the occurrences of impact melts. In: Roddy, D.J., Pepin, R.O., Merrill, R.B. (Eds.), Impact and Explosion Cratering. Pergamon Press, New York, pp. 791–814.

Gurov, E.P., Kelley, S.P., Koeberl, C., 2003. Ejecta of the Boltysh impact crater in the Ukrainian Shield. In: Koeberl, C., Martinez-Ruiz, F.C. (Eds.), Impact Markers in the Stratigraphic Record. Springer, Heidelberg, pp. 179–202.

Gurov, E., Gurova, E., Chernenko, Y., Yamnichenko, A., 2009. The Obolon impact structure, Ukraine, and its ejecta deposits. Meteorit. Planet. Sci. 44, 389–404.

Hawke, B.R., Head, J.W., 1977. Impact melt on lunar crater rims. In: Roddy, D.J., Pepin, R.O., Merrill, R.B. (Eds.), Impact and Explosion Cratering. Pergamon Press, New York, pp. 815–841.

Heiken, G., Vaniman, D., French, B.M., 1991. Lunar Sourcebook: A User's Guide to the Moon. Cambridge University Press, New York.

Hiesinger, H., Head III, J.W., 2006. New views of Lunar geoscience: an introduction and overview. Rev. Mineral. Geochem. 60, 1–81.

Hörz, F., 1965. Untersuchungen an Riesgläsern. Beitr. Mineral. Petrogr. 11, 621–661.

Hörz, F., 1982. Ejecta of the Ries crater, Germany. In: Silver, L.T., Schultz, P.H. (Eds.), Geological Implications of Impacts of Large Asteroids and Comets on the Earth. : Geological Society of America Special Paper, 190. Geological Society of America, Boulder, pp. 39–55.

Hörz, F., Ostertag, R., Rainey, D.A., 1983. Bunte breccia of the Ries: continuous deposits of large impact craters. Rev. Geophys. Space Phys. 21, 1667–1725.

Hörz, F., Mittlefehldt, D.W., See, T.H., Galindo, C., 2002. Petrographic studies of the impact melts from Meteor Crater, Arizona, USA. Meteorit. Planet. Sci. 37, 501–531.

Housen, K.R., Holsapple, K.A., 2011. Ejecta from impact craters. Icarus 211, 856–875.

Howard, K.A., Wilshire, H.G., 1975. Flows of impact melt at lunar craters. J. Res. U.S. Geol. Surv. 3, 237–251.

Ivanov, B.A., Artemieva, N., 2001. Transient cavity scaling for oblique impacts. Lunar Planet. Sci. 32 Abs. 1327.

Ivanov, B.A., Artemieva, N., 2002. Numerical modeling of the formation of large impact craters. In: Koeberl, C., MacLeod, K.G. (Eds.), Catastrophic Events and Mass Extinctions: Impacts and Beyond, Special Paper of the Geological Society of America 356. Geological Society of America, Boulder, pp. 619–630.

Kenkmann, T., Ivanov, B.A., 2000. Low-angle faulting in the basement of complex impact craters; numerical modelling and field observations in the Rochechouart Structure, France. In: Gilmour, I., Koeberl, C. (Eds.), Impacts and the Early Earth. : Lecture Notes in Earth Sciences, 91. Springer, Berlin, pp. 279–308.

Kenkmann, T., Ivanov, B.A., 2006. Target delamination by spallation and ejecta dragging: an example from the Ries crater's periphery. Earth Planet. Sci. Lett. 252, 15–29.

Kieffer, S.W., Phakey, P.P., Christie, J.M., 1976. Shock processes in porous quartzite: transmission electron microscope observations and theory. Contrib. Mineral. Petrol. 59, 41–93.

Komatsu, G., Ori, G.G., Di Lorenzo, S., Rossi, A.P., Neukum, G., 2007. Combinations of processes responsible for Martian impact crater "layered ejecta structures" emplacement. J. Geophys. Res. 112. doi:10.1029/2006je002787.

Kring, D.A., 2000. Impact events and their effect on the origin, evolution, and distribution of life. GSA Today 10, 1–7.

Mader, M., Osinski, G.R., Marion, C., 2011. Impact ejecta at the Mistastin Lake impact structure, Labrador. Lunar Planet. Sci. 41 Abs. 2505.

Maloof, A.C., Stewart, S.T., Weiss, B.P., Soule, S.A., Swanson-Hysell, N.L., Louzada, K.L., Garrick-Bethell, I., Poussart, P.M., 2010. Geology of Lonar Crater, India. Geol. Soc. Am. Bull. 122, 109–126.

Marvin, U.B., Kring, D.A., 1992. Authentication controversies and impactite petrography of the New Quebec crater. Meteoritics 27, 585–595.

Masaitis, V.L., 1999. Impact structures of northeastern Eurasia: the territories of Russia and adjacent countries. Meteorit. Planet. Sci. 34, 691–711.

Melosh, H.J., 1989. Impact Cratering: A Geologic Process. Oxford University Press, New York.

Mest, S.C., Weitz, C.M., Tornabene, L.L., 2011. Correlation of low-albedo deposits on the floors of Oudemans Crater and southest Noctis Labyrinthus. Lunar Planet. Sci. 42 Abs. 2547.

Meyer, C., Jébrak, M., Stöffler, D., Riller, U., in press. Lateral transport of suevite inferred from 3D shape fabric analysis: Evidence from the Ries impact crater, Germany. Geol. Soc. Am. Bull.

Miyamoto, H., Sasaki, S., 2000. Two differennt styles of crater outflow materials on Venus inferred from numericaal simulations over DEMs. Icarus 145, 533–545.

Monod, T., Pomerol, C., 1966. La cratère d'explosion de Tenoumaer (Mautitane) et ses laves. Bull. Geol. Soc. Fr. 7, 165–172.

Morris, A.R., Mouginis-Mark, P.J., Garbeil, H., 2010. Possible impact melt and debris flows at Tooting Crater, Mars. Icarus 209, 369–389.

Mouginis-Mark, P.J., Baloga, S.M., 2006. Morphology and geometry of the distal ramparts of Martian impact craters. Meteorit. Planet. Sci. 41, 1469–1482.

Newsom, H.E., Graup, G., Sewards, T., Keil, K., 1986. Fluidization and hydrothermal alteration of the suevite deposit in the Ries Crater, West Germany, and implications for Mars. J. Geophys. Res. B: Solid Earth Planets 91, 239–251.

Oberbeck, V.R., 1975. The role of ballistic erosion and sedimentation in lunar stratigraphy. Rev. Geophys. Space Phys. 13, 337–362.

Oberbeck, V.R., 2009. Layered ejecta craters and the early water/ice aquifer on Mars. Meteorit. Planet. Sci. 44, 43–54.

Osinski, G.R., 2004. Impact melt rocks from the Ries impact structure, Germany: an origin as impact melt flows? Earth Planet. Sci. Lett. 226, 529–543.

Osinski, G.R., Spray, J.G., 2005. Tectonics of complex crater formation as revealed by the Haughton impact structure, Devon Island, Canadian High Arctic. Meteorit. Planet. Sci. 40, 1813–1834.

Osinski, G.R., Grieve, R.A.F., Spray, J.G., 2004. The nature of the groundmass of surficial suevites from the Ries impact structure, Germany, and constraints on its origin. Meteorit. Planet. Sci. 39, 1655–1684.

Osinski, G.R., Spray, J.G., Lee, P., 2005. Impactites of the Haughton impact structure, Devon Island, Canadian High Arctic. Meteorit. Planet. Sci. 40, 1789–1811.

Osinski, G.R., Bunch, T.E., Wittke, J., 2006. Proximal ejecta at Meteor Crater, Arizona: discovery of impact melt-bearing breccias. Lunar Planet. Sci. 37 Abs. 1005.

Osinski, G.R., Grieve, R.A.F., Collins, G.S., Marion, C., Sylvester, P., 2008. The effect of target lithology on the products of impact melting. Meteorit. Planet. Sci. 43, 1939–1954.

Pernicka, E., Horn, P., Pohl, J., 1987. Chemical record of the projectile in the graded fall-back sedimentary unit from the Ries Crater, Germany. Earth Planet. Sci. Lett. 86, 113–121.

Pierazzo, E., Melosh, H.J., 2000. Melt production in oblique impacts. Icarus 145, 252–261.

Pope, K.O., Kieffer, S.W., Ames, D.E., 2006. Impact melt sheet formation on Mars and its implication for hydrothermal systems and exobiology. Icarus 183, 1–9.

Pratesi, G., Morelli, M., Rossi, A.P., Ori, G.G., 2005. Chemical compositions of impact melt breccias and target rocks from the Tenoumer impact crater, Mauritania. Meteorit. Planet. Sci. 40, 1653–1672.

Prockter, L.M., Ernst, C.M., Denevi, B.W., Chapman, C.R., Head, J.W., Iii, Fassett, C.I., Merline, W.J., Solomon, S.C., Watters, T.R., Strom, R.G., Cremonese, G., Marchi, S., Massironi, M., 2010. Evidence for young volcanism on Mercury from the third MESSENGER flyby. Science 329, 668–671.

Rogers, A.D., Christensen, P.R., Bandfield, J.L., 2005. Compositional heterogeneity of the ancient Martian crust: analysis of Ares Vallis bedrock with THEMIS and TES data. J. Geophys. Res. 110. doi:10.1029/2005JE002399.

Salge, T. (2007) The ejecta blanket of the Chicxulub impact crater, Yucatán, Mexico: Petrographic and chemical studies of the K-P section of El Guayal and UNAM boreholes. Ph.D. Thesis, Humboldt University, Berlin.

Scherler, D., Kenkmann, T., Jahn, A., 2006. Structural record of an oblique impact. Earth Planet. Sci. Lett. 248, 43–53.

Schönian, F., Stöffler, D., Kenkmann, T., 2004. The fluidized Chicxulub ejecta blanket, Mexico: implications for Mars. Lunar Planet. Sci. 35 Abs. 1848.

Schultz, P.H., 1993. Impact crater growth in an atmosphere. Int. J. Impact Eng. 14, 659–670.

Schultz, P.H., Gault, D.E., 1979. Atmospheric effects on martian ejecta emplacement. J. Geophys. Res. 84, 7669–7687.

Shoemaker, E.M., 1963. Impact mechanics at Meteor Crater, Arizona. In: Middlehurst, B.M., Kuiper, G.P. (Eds.), The Moon, Meteorites and Comets. University of Chicago Press, Illinois, pp. 301–336.

Shuvalov, V., 2003. Cratering process after oblique impacts. Third Int. Conf. Large Meteorite Impacts, Abs. 4130.

Stewart, S.T., Ahrens, T.J., 2005. Shock properties of H_2O ice. J. Geophys. Res. 110, E03005. doi:10.1029/2004JE002305, 2005.

Stöffler, D., 1977. Research drilling Nördlingen 1973: polymict breccias, crater basement, and cratering model of the Ries impact structure. Geol. Bav. 75, 443–458.

Stöffler, D., Grieve, R.A.F., 2007. Impactites. In: Fettes, D., Desmons, J. (Eds.), Metamorphic Rocks. Cambridge University Press, Cambridge, pp. 82–92.

Stöffler, D., Gault, D.E., Wedekind, J., Polkowski, G., 1975. Experimental hypervelocity impact into quartz sand: distribution and shock metamorphism of ejecta. J. Geophys. Res. 80, 4062–4077.

Stöffler, D., Artemieva, N.A., Pierazzo, E., 2002. Modeling the Ries-Steinheim impact event and the formation of the moldavite strewn field. Meteorit. Planet. Sci. 37, 1893–1907.

Strom, R.G., Croft, S.K., Barlow, N.G., 1992. The Martian impact cratering record. In: Kieffer, H.H., Jakosky, B.M., Snyder, C.W., Matthews, M.S. (Eds.), Mars. University of Arizona Press, Tucson, pp. 383–423.

Suzuki, A., Kumagai, I., Nagata, Y., Kurita, K., Barnouin-Jha, O.S., 2007. Modes of ejecta emplacement at Martian craters from laboratory experiments of an expanding vortex ring interacting with a particle layer. Geophys. Res. Lett. 34. doi:10.1029/2006GL028372.

Tong, C.H., Lana, C., Marangoni, Y.R., Elis, V.R., 2010. Geoelectric evidence for centripetal resurge of impact melt and breccias over central uplift of Araguainha impact structure. Geology 38, 91–94.

Tornabene, L.L., Mcewan, A.S., Osinski, G.R., Mouginis-Mark, P., Boyce, J.M., Williams, R.M.E., Wray, J.J., Grant, J.A., 2007. Impact melting and the role of sub-surface volatiles: implications for the formation of valley networks and phyllosilicate-rich lithologies on Early Mars. Seventh Int. Conf. Mars, Abs. 3288.

Tornabene, L.L., Moersch, J.E., Mcsween Jr., H.Y., Hamilton, V.E., Piatek, J.L., Christensen, P.R., 2008. Surface and crater-exposed lithologic units of the Isidis Basin as mapped by coanalysis of THEMIS and TES derived data products. J. Geophys. Res. 113. doi:10.1029/2007JE002988.

Turtle, E.P., Pierazzo, E., Collins, G.S., Osinski, G.R., Melosh, H.J., Morgan, J.V., Reimold, W.U., 2005. Impact structures: what does crater diameter mean? In: Kenkmann, T., Hörz, F., Deutsch, A. (Eds.), Large meteorite impacts III. : Geological Society of America Special Paper, 384. Geological Society of America, Boulder, pp. 1–24.

Vishnevsky, S.A., Lagutenko, V.N., 1986. The Ragozinka astrobleme: an Eocene crater in central Urals (in Russian). Akad. Nauk USSR 14, 1–42.

Wada, K., Barnouin-Jha, O.S., 2006. The formation of fluidized ejecta on Mars by granular flows. Meteorit. Planet. Sci. 41, 1551–1569.